

Ionospheric midlatitude electric current density inferred from multiple magnetic satellites

Rob Shore¹, Kathy Whaler¹, Susan Macmillan², Ciaran Beggan², Nils Olsen³, Tim Spain⁴, Anasuya Aruliah⁴

Authors' affiliation: ¹: University of Edinburgh, ²: British Geological Survey, ³: DTU Space, ⁴: University College London
Contact email of first author: robore@bas.ac.uk



Motivation and aims

Satellites in low-Earth orbit fly through the magnetised plasma of the ionosphere, in which a complex array of electric currents flow in both the day and night sectors. The currents contribute to the measured magnetic field, violating the assumption of measurement in a source-free region – a requirement of magnetic field representations which adopt a scalar potential. Data selection techniques (e.g. selecting only nightside data) are commonly employed to lessen the effect of these unwanted magnetic contributions, necessitating a detailed understanding of the distribution and magnitudes of the currents. We use near-simultaneous overflights of the Ørsted and CHAMP satellites to define a closed circuit for an application of Ampère's integral law to magnetic data, in order to estimate total current flow in the region between the two orbital paths. We present trends in the zonal mid-latitude ionospheric electric current density at a range of local times (LT) and phases of the solar cycle.

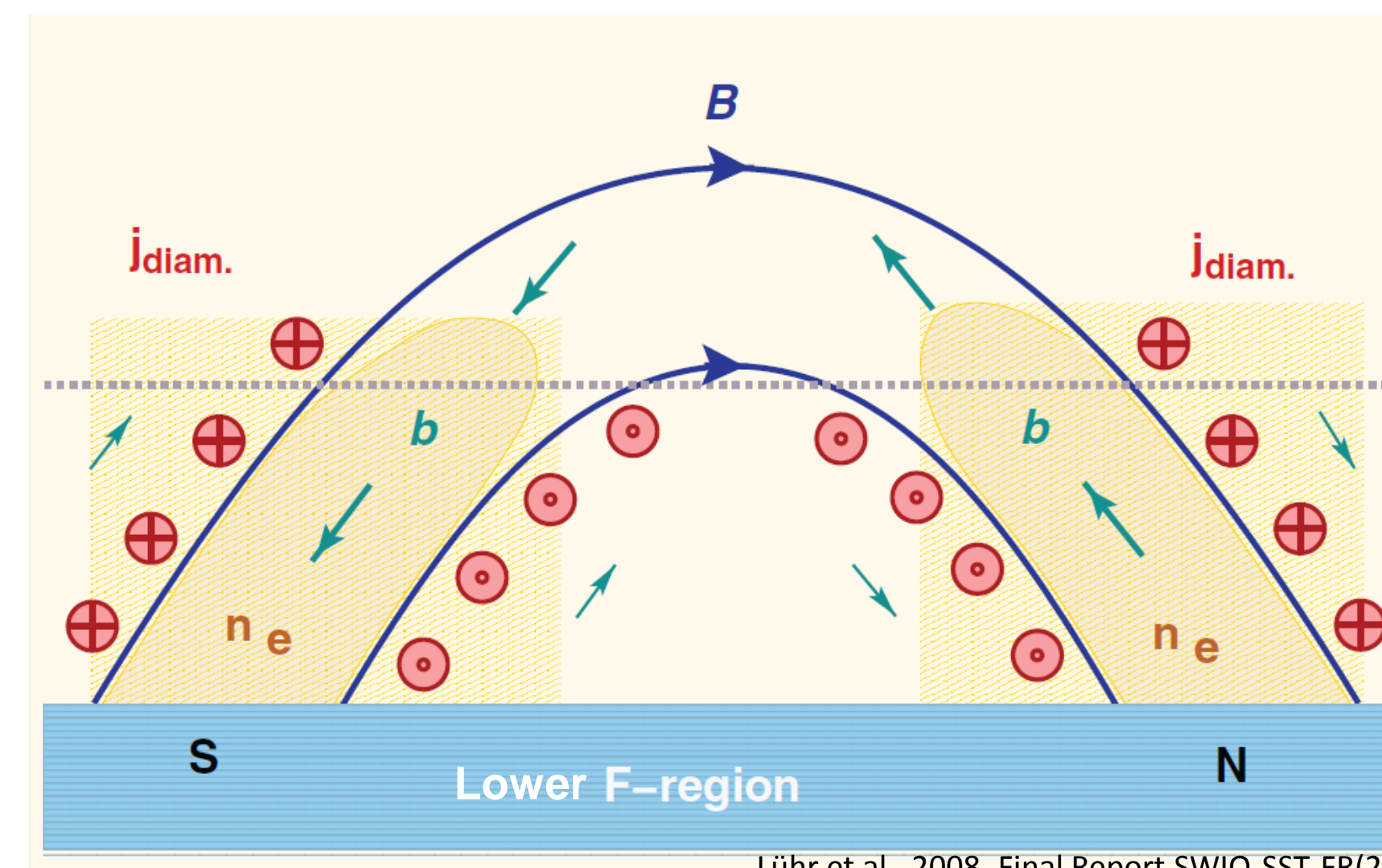


Fig 1: North-south cross-section through equatorial ionisation anomaly (of increased plasma density) entrained in magnetic field lines B, and host to diamagnetic currents j.

Lühr et al., 2008, Final Report SWIO-SST-FR(2); ESTEC Contract No. 20943/07/NL/JA, ESA

Method

Orbits of Ørsted and CHAMP

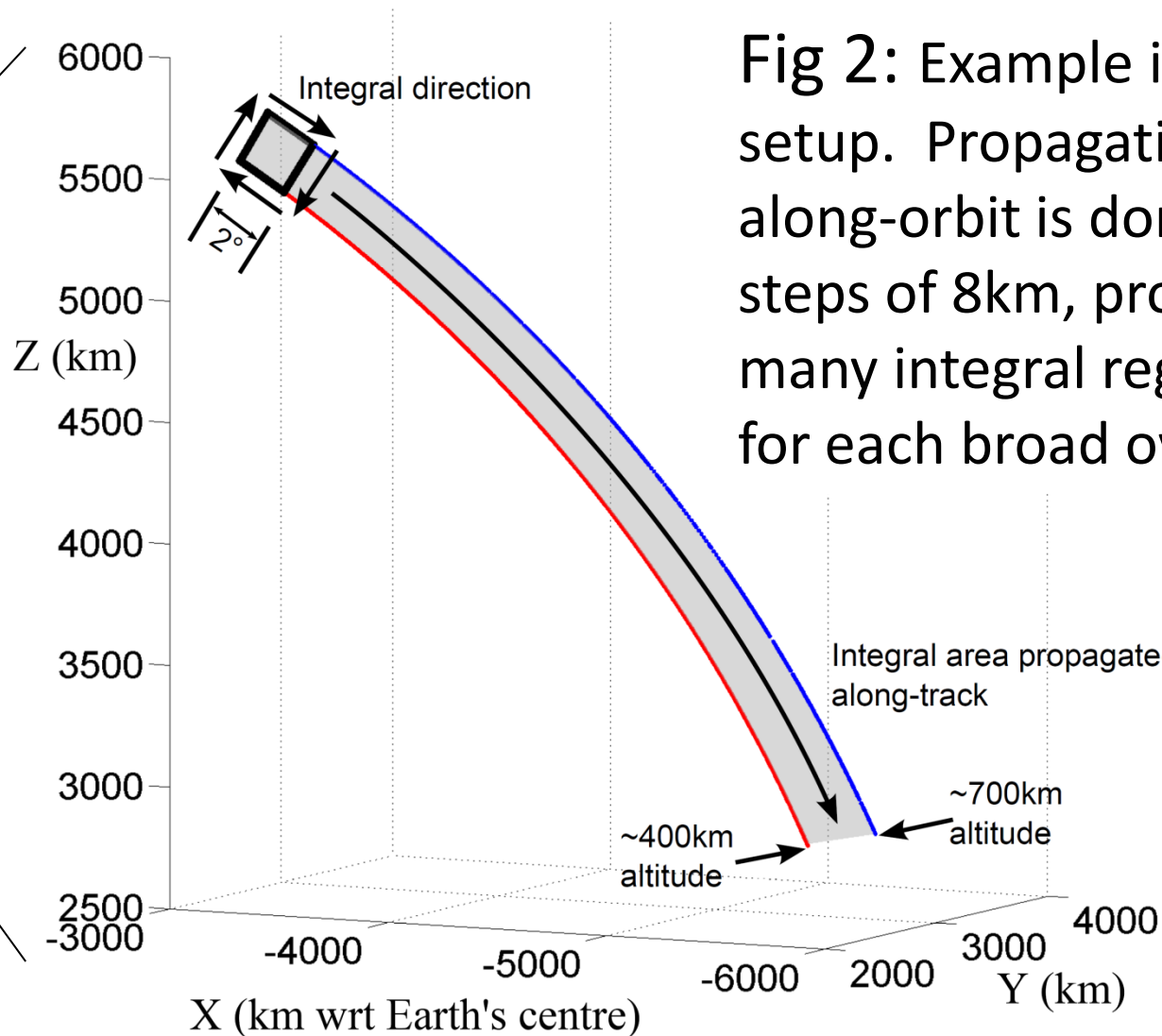
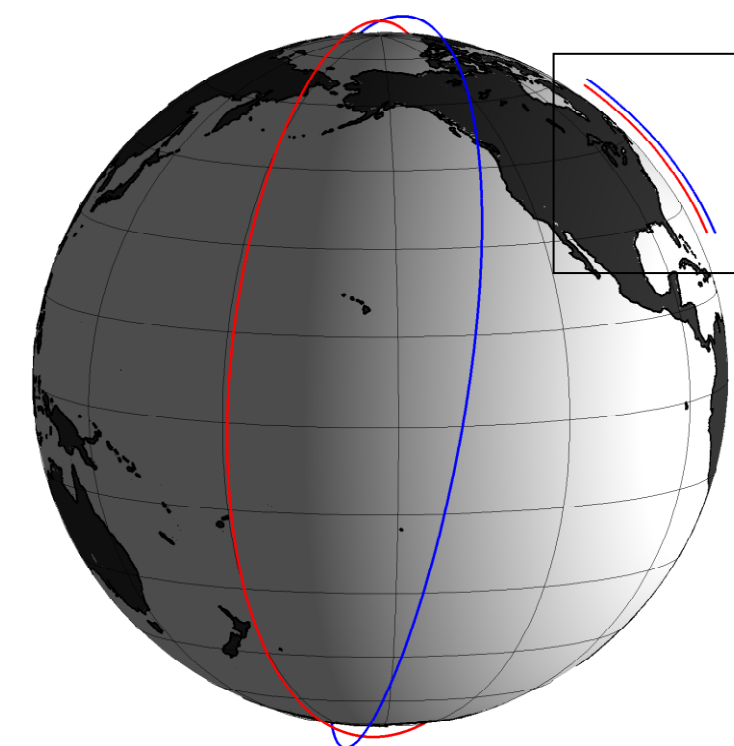


Fig 2: Example integral setup. Propagation along-orbit is done in steps of 8km, producing many integral regions for each broad overlap.

The corrected magnetic vector values $\Delta \mathbf{B}$ are rotated to the (inertial) along-track frame, and the integral contribution values are calculated for each line element $d\mathbf{l}$ in the integral loop via the dot product. The sum of these individual current contributions is divided by the area A enclosed by the two satellite tracks to produce the current density J flowing normal to the integral loop;

$$J = \frac{\sum_{i=1}^n \Delta \mathbf{B}_{ATi} \cdot d\mathbf{l}_{ATi}}{\mu_0 A}$$

where n is the number of line elements in the integral circuit, μ_0 is the permeability of free space, and the subscript 'AT' indicates vectors in the along-track frame. The integral loop is then incremented by one measurement point along-track (e.g. Fig 2), and the process repeated. Mutually available vector magnetic data in the period 2000-2006 (shown in Fig 3) allows overlaps spanning the full 24-hour range of LTs twice (in discrete overlap epochs). The vast majority of these overlaps are rejected as they overlap closely in space, but not in time.

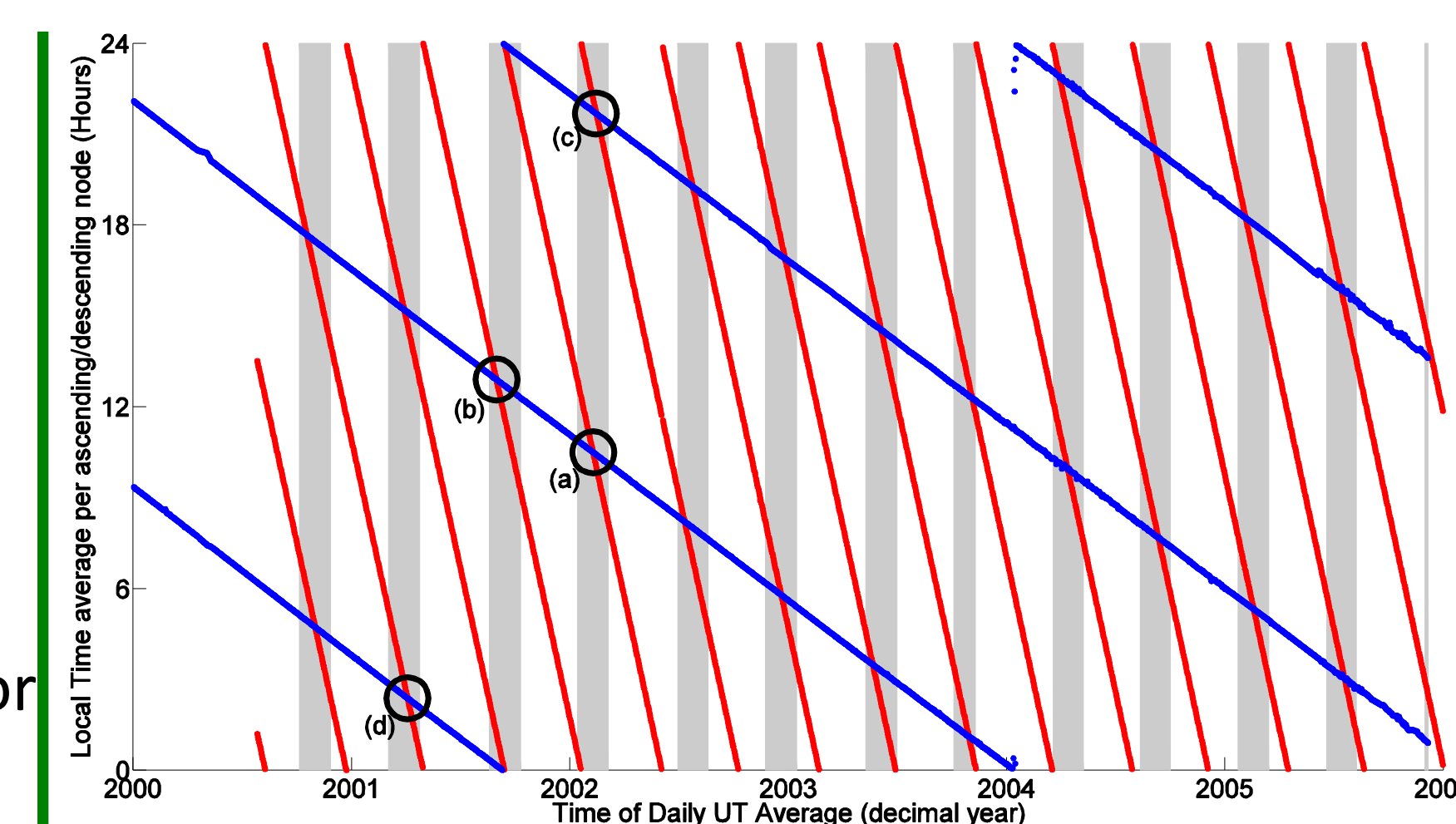
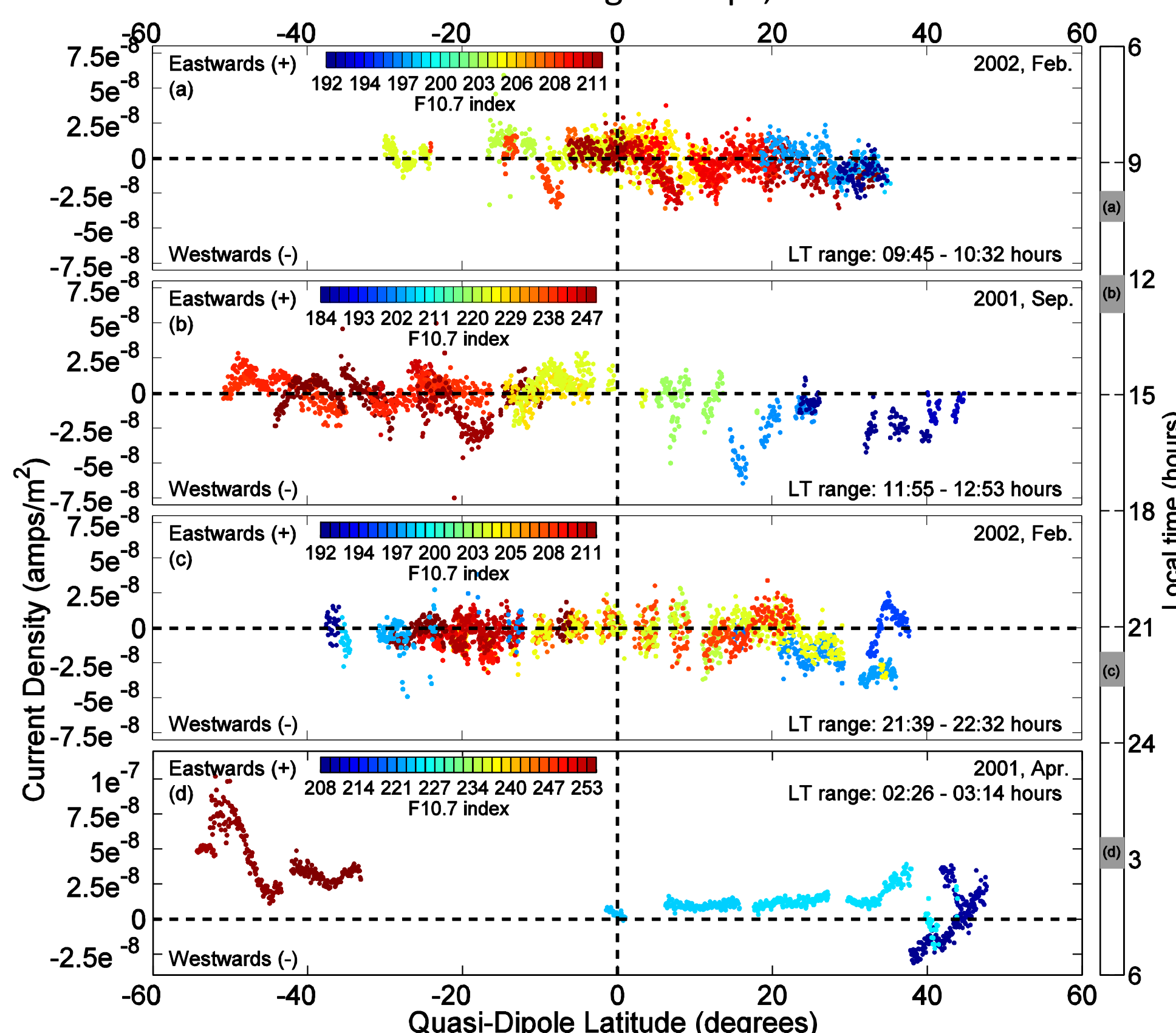


Fig 3: Daily local time (LT) averages at mid-latitude for the ascending and descending nodes of the Ørsted (blue) and CHAMP (red) satellites. Shaded regions indicate 2 hours LT proximity of CHAMP to Ørsted. Circles are sectors of Figs 4&5.

After correcting the magnetic data for estimates of the core and crustal fields, the integral loop is formed from two arcs of data each 2 degrees colatitude in length, equal to the minimum radial spacing between the two orbits. The radial connecting elements of the circuit have no data coverage between their endpoints, but still represent a part of the loop bridging two measurement points as we treat the radial elements in an identical manner to the line elements formed along the satellite tracks.

Results

Fig 4: Current density estimates resulting from individual integral loops, shown in 4 sectors of LT.



We do not have current density estimates at all LTs as a continuous data set, since the usable data are recorded at times months apart, in different geomagnetic conditions and at different points in the solar cycle. However, the specific trends shown in Figure 4 and discussed here all occur in more than one overlap epoch and exhibit similar forms at different geomagnetic, seasonal and solar conditions. Thus, the trends discussed here are considered representative of the electrodynamic of the upper F-region ionosphere at the set of LTs shown. Some systematic, global-scale features of the current density estimates shown in Figure 4 are as follows. On the dayside the estimated current flow is strongest in the westwards direction, and has higher magnitude than on the nightside. In terms of latitude, the dayside current density is stronger near the dip equator than towards the poles (appearing to follow the Appleton anomaly distribution). On the nightside, the current has no strong direction preference, has much lower magnitudes and exhibits weak latitudinal trends until after midnight, when the current density is strongest in the mid-latitudes. This combination of latitude and LT was typically considered to be relatively free of currents, and the presence of these intensifications was not expected – their cause remains an open issue. The magnitude of the current density estimates all lie within the range $\pm 0.1 \mu\text{A}/\text{m}^2$. The values in Figure 4 are coloured by samples of the F10.7 index of solar flux density. The solar flux appears to have minimal effect on the current density estimates – the same is true for the Dst index level.

Current density estimates from individual overlaps in 4 LT sectors

Model comparison of current density estimates in 4 LT sectors

Of the factors which can control the magnitude of our results (solar activity, geomagnetic activity, season and longitude sector), none impacts significantly on the trends discussed. However, we can only resolve the average current density and cannot distinguish between the separate contributing current sources in the satellite data. Hence, an independent validation of the broad-scale spatio-temporal trends in the Ørsted/CHAMP estimates is desirable. In Figure 5 we compare the Ørsted/CHAMP results to predictions of the Lorentz, gravity and pressure gradient currents from CTIP (Coupled Thermosphere-Ionosphere-Plasmasphere), a self consistent, first-principles, 3-dimensional numerical model of ionospheric composition and temperatures. Note that the CTIP current densities have been (arbitrarily) multiplied by a uniform factor of 2 to aid in comparisons with the results from Ørsted and CHAMP. The CTIP model prediction is dependent on the sum of several competing sources of current. Typically, where these sources diverge most strongly, the Ørsted/CHAMP estimates have their highest magnitudes. A notable exception to this is that the CTIP predictions in Figure 5(a) and (b) show the Appleton anomaly in a non-bifurcated form, suggesting that the development of this structure is more rapid than is parametrised in the model.

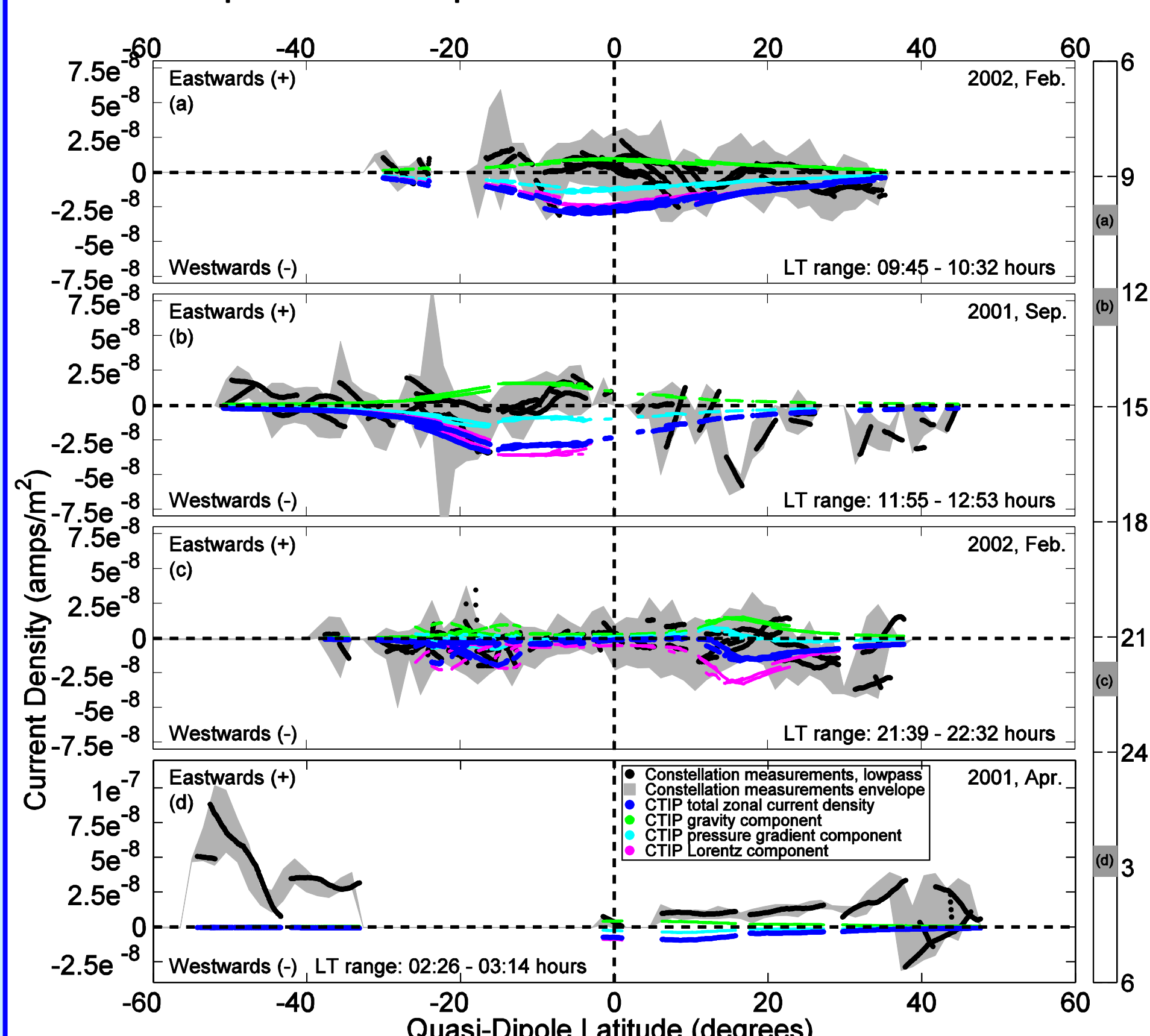


Fig 5: Fig 4 overlaps with current density estimates shown as smoothed values with an envelope, and CTIP model predictions

Effect of missing radial data

Here we test the effect of the lack of data within the radial line elements of the integral loop. Synthetic CTIP current density values were sampled to two location sets: 'sparse' loops, which are true to the real data distribution, and 'dense' loops, which have uniformly distributed values around the integral loop. The current density values were used in an application of the Biot-Savart law to predict the magnetic effect of the synthetic current (I_{syn}) at the data locations:

$$\mathbf{B}_{syn} = \frac{\mu_0 I_{syn} \hat{s}}{2\pi r}$$

where \mathbf{B}_{syn} is the magnetic effect (at a certain location) of the enclosed synthetic current I_{syn} , \hat{s} is a unit vector in the direction of the magnetic field which results from a current flowing through an infinite-length thin wire at the centre of the integral loop, aligned in the direction normal to the plane of the enclosed area, and r is the length of a vector connecting the centre of the integral loop to the point at which \mathbf{B}_{syn} is predicted. The \mathbf{B}_{syn} values were used in the Ampère's integral method, and the recovered current density was compared to the synthetic input.

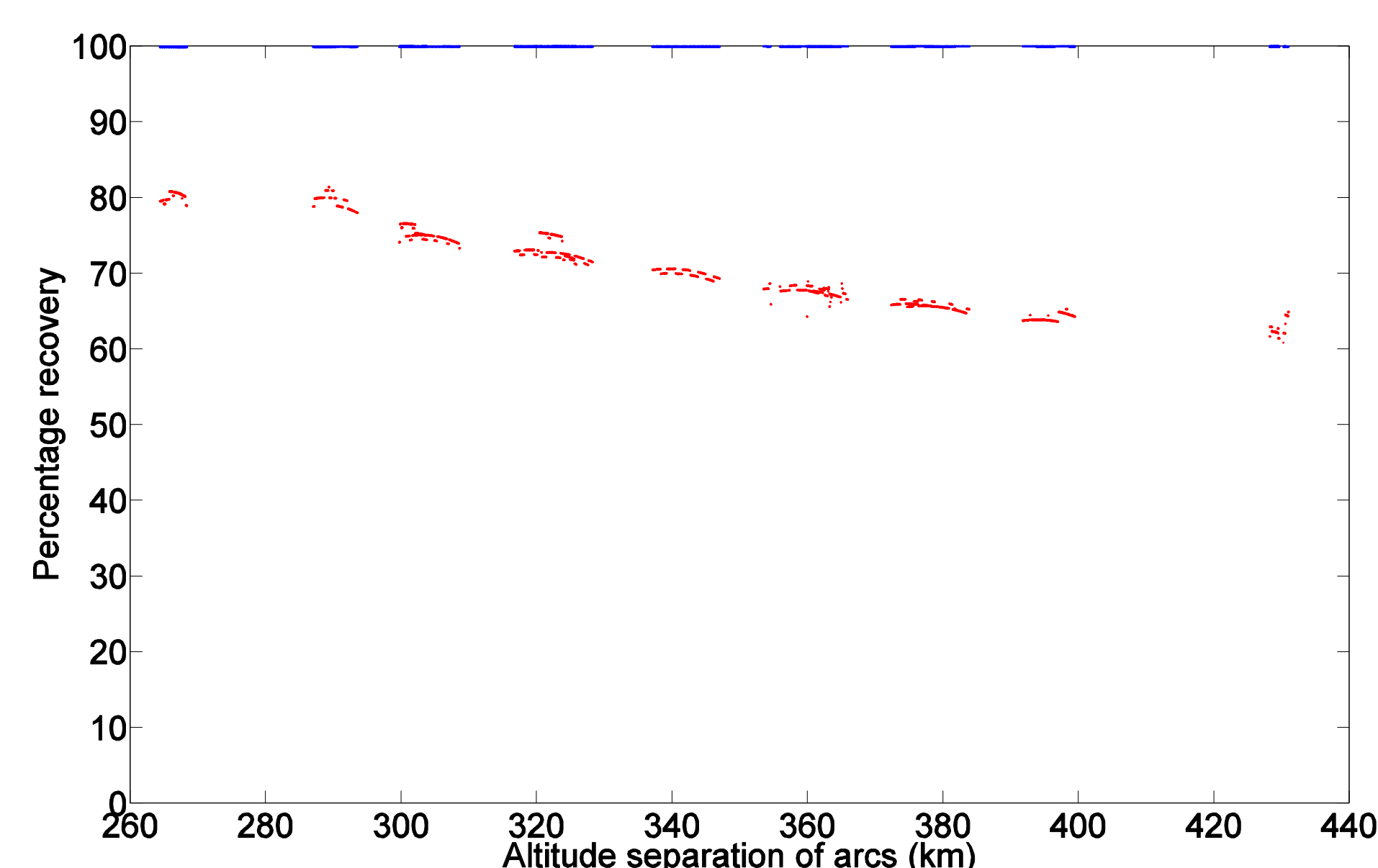


Fig 6: Recovery proportion for dense (blue) and sparse (red) loops. The proportion varies predictably with altitude separation.

As shown in Figure 6, the dense loop recovery proportion is near 100%, and the sparse loop recovery proportion varies between 80 and 60%, dependent upon the altitude separation of the Ørsted and CHAMP satellites. The sparse loop recovery is representative of the case for the real data, and hence the results presented in Figures 4 and 5 are expected to be underestimates, by $\sim 30\%$.